

# NCRF: Neural Contact Radiance Fields for Free-Viewpoint Rendering of Hand-Object Interaction

Zhongqun Zhang<sup>1,2\*</sup>Jifei Song<sup>2†</sup>Eduardo Pérez-Pellitero<sup>2</sup>Yiren Zhou<sup>2</sup>Hyung Jin Chang<sup>1</sup>Aleš Leonardis<sup>1,2</sup><sup>1</sup>University of Birmingham, UK    <sup>2</sup>Huawei, Noah's Ark Lab

zxz064@student.bham.ac.uk, {jifeisong, e.perez.pellitero, zhouyiren}@huawei.com

{h.j.chang, a.leonardis}@bham.ac.uk

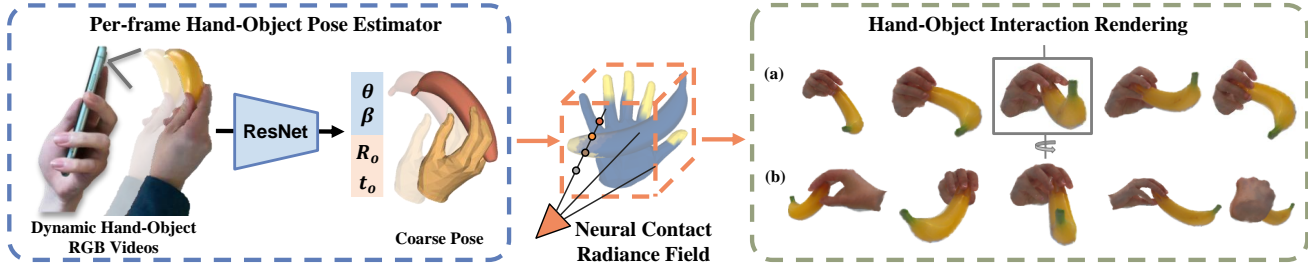


Figure 1. Given RGB videos of dynamic hand-object interaction and coarse hand-object poses generated by a pose estimator, NCRF models (a) hand-object movement with photo-realistic appearance, which can be used for (b) free-viewpoint rendering for any frame (e.g. frame highlighted in the gray square) in a sequence.

## Abstract

Modeling hand-object interactions is a fundamentally challenging task in 3D computer vision. Despite remarkable progress that has been achieved in this field, existing methods still fail to synthesize the hand-object interaction photo-realistically, suffering from degraded rendering quality caused by the heavy mutual occlusions between the hand and the object, and inaccurate hand-object pose estimation. To tackle these challenges, we present a novel free-viewpoint rendering framework, Neural Contact Radiance Field (NCRF), to reconstruct hand-object interactions from a sparse set of videos. In particular, the proposed NCRF framework consists of two key components: (a) A contact optimization field that predicts an accurate contact field from 3D query points for achieving desirable contact between the hand and the object. (b) A hand-object neural radiance field to learn an implicit hand-object representation in a static canonical space, in concert with the specifically designed hand-object motion field to produce observation-to-canonical correspondences. We jointly learn these key

components where they mutually help and regularize each other with visual and geometric constraints, producing a high-quality hand-object reconstruction that achieves photo-realistic novel view synthesis. Extensive experiments on HO3D and DexYCB datasets show that our approach outperforms the current state-of-the-art in terms of both rendering quality and pose estimation accuracy.

## 1. Introduction

Understanding and modeling hand-object interactions, as well as the reconstruction and manipulation, play an important role in interpreting human activities and behaviors [4, 9, 14–16, 19, 21, 26, 39, 46]. It is of particular interest for various of promising applications in human-computer interaction [36, 42], AR/VR [17, 33], and imitation learning in robotics [10, 34]. Previous works typically formulate this task as a joint hand and object pose estimation problem [9, 15, 23] and rely on parametric hand-object models such as MANO [35] and YCB [3] to estimate the hand motion transformation. Even though hand parametric models like MANO can bring strong prior knowledge of the shape information, existing methods struggle to recover the de-

\*This work was developed while interning at Huawei.

†Corresponding author.

tails and are limited to a lower resolution. One of the latest approaches, NIMBLE [25], further shows improved skin details over MANO but requires expensive scan data and annotation to generate a personalized and photo-realistic appearance.

The direction of neural rendering sheds light on the photo-realistic novel view synthesis. Neural Radiance Field (NeRF) [28] proposed to learn implicit neural representations, with the integration of position encoding and volumetric rendering, showing huge potential for high-quality novel-view synthesis and fine-grained detail reconstruction. NeRF has later been adapted to represent dynamic human body [20, 30, 31, 37, 38, 44], achieving compelling results on modeling a clothed human. Similarly, leveraging head parametric models like FLAME, 3D head avatar creation approaches [1, 18, 45] built on NeRF also show high-quality facial appearance and geometry. In terms of hand modeling, LISA [8] is the first neural rendering model that can capture the accurate shape and appearance of human hands from multi-view images. The hand reconstruction quality has been further improved by the following work [6]. However, how the hand is interacting with the outside world, specifically hand-object interaction is not yet considered in the light of neural rendering. Existing dynamic NeRF methods [30, 44] also fail to apply to hand-object interaction, due to the complex motion involved in human hand grasping objects, and heavy mutual occlusions frequently happening between hand and objects. Moreover, the visual and geometric prior of contact information is of critical importance but is unfortunately ignored in the previous neural hand approaches.

To address the aforementioned challenges, we propose Neural Contact Radiance Field (NCRF), where we focus on the problem of free-viewpoints rendering for hand-object interactions using RGB videos, as illustrated in Fig. 1. Our method can work on multi-view video captured by hardware-synchronized industrial cameras in the lab setting, like DexYCB Dataset [5], and more importantly, can also work with monocular video taken from mobile phones in a casual way, making our pipeline widely applicable to hand-held mobile devices. To model and reconstruct the realistic details of the hand-object interaction, we build a novel dynamic hand-object neural radiance field that learns an implicit neural representation of hand-object interactions in canonical space, wherein a specifically designed hand-object motion field is incorporated to build observation-to-canonical correspondence, combining both skeletal and non-rigid motion for the hand, as well as the rigid motion transformation for the object. In addition, to further improve the hand-object pose estimation, we design a novel contact optimization field that refines the initial coarse hand-object poses from an off-the-shelf image-based pose estimator [15], where we first estimate a contact field between hand and object by introducing an attention mechanism to model the interaction

cues of 3D hand-object query points, and then constrain the hand-object pose with the desired contact prior. Lastly, to solve the challenges introduced by heavy mutual occlusion when hands often inevitably intersect with the object, we introduce a mesh-guided ray sampling strategy to mitigate the blurriness caused by hand-object intersection. We jointly optimize the contact optimization field and the neural radiance field using contact and photo-metric loss and observed that both hand-object interaction modeling and hand-object pose estimation can benefit each other, and achieve high-quality hand-object reconstruction performance.

To the best of our knowledge, we are the first to propose a free-viewpoint rendering system based on NeRF for hand-object interactions. We evaluate our approach on the HO3D [12] and DexYCB [5] datasets that capture hand-object interactions in complex motions. Across all video sequences, our approach exhibits state-of-the-art performances on free-viewpoint rendering and shows significant improvements in hand-object pose optimization. In summary, our contributions are three-fold:

- We propose a novel dynamic hand-object neural radiance field capable of modeling complex hand-object interactions with mutual occlusions between hand and object, achieving high-quality hand-object reconstructions and photo-realistic novel view rendering.
- To further improve the modeling of hand-object interaction, we propose a novel attention-based network for estimating the hand-object contact field and optimizing both hand and object poses, and the refined pose will further benefit the hand-object neural rendering under joint learning.
- Extensive experiment results on HO3D and DexYCB show that our method outperforms the state-of-the-art both quantitatively and qualitatively, in terms of both hand-object rendering quality and hand-object pose estimation accuracy.

## 2. Related work

Our work tackles the problem of hand-object interaction from a sparse set of videos. We first give the literature review on modeling hand-object interaction. Then we review the human-centric neural rendering. To this end, we briefly cover the methods using the contact information for hand-object pose refinement.

**Hand-object interaction.** modeling hand-object interaction is of promising application value yet challenging to solve due to severe occlusion between hand and object. Earlier work by Hasson *et al.* [14] gave the first attempt by jointly regressing MANO hand parameters [35] and reconstructing object mesh with physical constraints, showing improved grasping quality. Most works [4, 11, 13, 15, 23, 26, 41, 46, 48, 50] assume the object models is known and estimate the 6D object pose instead. Leveraging the spatial-

temporal consistency, Liu *et al.* [26] boosts the estimation performance through contextual reasoning to extract interaction cues in time. Other works focus on inferring the shape and pose of the hand-held object agnostically by lifting the object template constraints [7, 15, 40, 47]. For example, Chen *et al.* [7] reconstructs hand-object shapes by combining SDFs and parametric representation and demonstrates the aligned SDF model reconstructs better shape details. Though existing approaches have shown improved hand grasping and object manipulation, the hand-object interaction modeling results lack the desired photo-realistic appearance information. In contrast, our work can recover the high-quality appearance as well as the detailed shape information.

**Human-centric neural radiance field.** Neural Radiance Field (NeRF) [28] is capable of synthesizing photo-realistic novel views of a static scene from multi-view images by learning an implicit representation. Further explorations [20, 30, 31, 37, 38, 44] adapt NeRF to deformable humans. NeuralBody [31] proposes to integrate structured latent code diffused from SMPL meshes into the neural radiance field for dynamic human modeling. Furthermore, Peng *et al.* [30] and Weng *et al.* [44] learn implicit body representation in a canonical T-pose space and learned blend weights are applied with 3D human skeletons to generate observation-to-canonical correspondences. To improve the generalization ability of neural human reconstruction, Key-pointNeRF [27] takes use of relative 3D spatial information from sparse key points. Specific to human hand modeling, LISA [8] chooses the skeleton model parameterized by MANO and predicts the color and density from the learned implicit function. Chen *et al.* [6] extent MANO to MANO-HD and generate high-fidelity appearance from the neural radiance field learned from monocular videos. However, existing human-centric neural rendering methods ignore the hand-object interaction, leaving the challenging task of modeling complex interactions between hand and object within the neural radiance field unresolved.

**Contact optimization.** Contact optimization is one important auxiliary task for hand-object interaction. ContactOpt [11] has shown that by estimating contact regions on the object, hand pose estimation can be further improved in hand-object tracking. S2Contact [41] leverages the annotated contact map together with free-generated pseudo contact information under the semi-supervised learning framework, demonstrating better generalization ability across datasets. Recently, TOCH [50] is also built on contact optimization and further introduces a temporal denoising auto-encoder to generate plausible grasping sequences. In this work, we propose a novel attention-based mechanism to encode the contact information and incorporate contact optimization in learning a more accurate motion transformation for both hand and object, which will be beneficial to the implicit neural representation learning for hand-object interaction.

### 3. Method

Given a sparse set of videos of hand-object interaction, our task is to generate a free-viewpoint video of the scene of hand-object interaction and optimize the poses of hand and object simultaneously. Without loss of generality, for each frame, we extract the foreground hand-object mask and apply it to filter out the background image pixels. We also initialize per-frame hand-object pose and mesh using an image-based off-the-shelf pose and shape estimator [15].

The overview of our approach is shown in Fig. 2, where we propose a novel hand-object neural radiance field to model the interaction between the hand and objects. We first propose the hand-object neural radiance field to model the hand-object interaction (Sec. 3.1). Moreover, a mesh-guided sampling method is used to separate the hand and object 3D query points based on the hand-object poses and mesh. To this end, we discuss how to estimate the contact field to refine the hand-object poses with a differentiable contact optimizer (Sec. 3.2), which will be jointly learned with the hand-object neural radiance field.

#### 3.1. Hand-Object Neural Radiance Field

NeRF [28] models the continuous radiance field of a static scene by learning an implicit neural function. As shown in Fig. 2, we further extend the neural radiance field to model the dynamic hand-object interaction. Specifically, for a given 3D point sampled from the scene of hand-object interaction, and a viewing direction as the input, our hand-object neural radiance field will be able to render the color and reconstruct the density. We first define the canonical volume,  $F_c$ , for the hand-object interaction:

$$F_c : (\mathbf{x}_c, \mathbf{d}, \psi_i) \mapsto (\mathbf{c}, \sigma), \quad (1)$$

where  $\mathbf{x}_c$  is the sampled 3D points from either hand or object along the ray direction in the canonical space. For each 3D point, it takes a spatial position  $\mathbf{x}$  and viewing direction  $\mathbf{d}$  as input to a neural network and outputs color  $\mathbf{c}$  and volume density  $\sigma$ . Here we also include the latent appearance code for the  $i$ -th frame,  $\psi_i$ , following NeRFies [29]. The function  $F_c$  is modeled by a multi-layer perceptron (MLP) network, which is trained from a set of RGB images of a hand-object interaction scene captured with different poses.

We then define a hand-object deformation field  $T$  to build the corresponding mapping for the 3D points between observation and canonical space on top of the hand-object pose. Thus, we can obtain the observation volume  $F_o$  by warping the canonical volume  $F_c$  with deformation field  $T$ :

$$F_o(\mathbf{x}, \mathbf{d}, \psi_i) = F_c(T(\mathbf{x}, \mathbf{P}), \mathbf{d}, \psi_i), \quad (2)$$

where predicting the color  $\mathbf{c}$  and density  $\sigma$  for sampled 3D hand-object points  $\mathbf{x}$  in observation space using observation volume  $F_o$ , is then converted to obtain the color and density

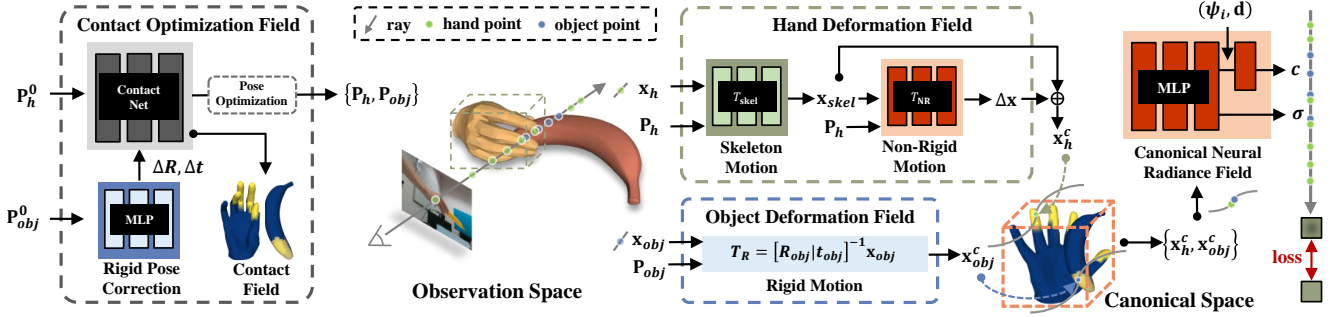


Figure 2. NCNF pipeline. We propose a novel hand-object neural radiance field to model the hand-object interaction. Our framework is composed of 1) a contact optimization field, leveraging contact prior in order to refine the hand-object pose, 2) a hand deformation field to deform hand points from observation to canonical space, considering both the skeletal and non-rigid motion, 3) object deformation field, which transforms the object into canonical space using refined rigid object pose, and 4) the canonical neural radiance field to build canonical volume for hand-object interaction and predict color and density.

of the corresponding point in canonical volume  $F_c$ , and  $T$  deforms 3D points from observation to canonical space, guided by the hand-object pose  $\mathbf{P}$ .

**Hand-object deformation field.** The motion transformation in the hand-object interaction is composed of hand skeleton motion, hand non-rigid motion, and object rigid motion. Therefore, we decompose the complex hand-object deformation field into the following parts:

$$T(\mathbf{x}, \mathbf{P}) = \begin{cases} T_{\text{skel}}(\mathbf{x}, \mathbf{P}_h) + T_{\text{NR}}(\mathbf{x}, \mathbf{P}_h), & \text{if } \mathbf{x} \in \mathbf{X}_h \\ T_{\text{R}}(\mathbf{x}, \mathbf{P}_{\text{obj}}), & \text{if } \mathbf{x} \in \mathbf{X}_{\text{obj}} \end{cases} \quad (3)$$

where  $T_{\text{skel}}$  provides the hand skeleton deformation, driven by refined hand pose  $\mathbf{P}_h$ , while  $T_{\text{NR}}$  describes the non-rigid movement for hand points  $\mathbf{X}_h$ .  $T_{\text{R}}$  provides rigid object deformation for object points  $\mathbf{X}_{\text{obj}}$ , driven by refined 6D object pose  $\mathbf{P}$ . Accurately separating 3D points into hand and object points is important, as the hand-object deformation falls into different motion fields of either hand or object. We, therefore, proposed a mesh-guided ray sampling strategy to indicate whether sampled points belong to hands or objects.

In particular, we first construct the hand deformation field based on the 3D hand skeleton. To map hand points from observation to canonical space, we compute the skeleton transformation using linear blend skinning algorithm [22]:

$$T_{\text{skel}}(\mathbf{x}, \mathbf{P}_h) = \sum_{i=1}^K w_o^i(\mathbf{x})(R_i \mathbf{x} + t_i) \quad (4)$$

where  $w_o^i$  is the blend weight for the  $i$ -th bone in observation space.  $R_i$  and  $t_i$  are rotation and translation for the  $i$ -th bone, respectively, which can be explicitly computed from hand pose  $\mathbf{P}_h$  [35]. Following the HumanNeRF [44], we use a CNN to learn blend weights  $\mathbf{W}_c$  in canonical space, from which we can derive  $w_o^i$  (see supplementary).

Furthermore, we build an additional non-rigid deformation field via MLP to model free-form shape deformation,

e.g., the deformation of fingertips due to pressure. It learns an offset  $\Delta x$  for  $\mathbf{x}_{\text{skel}}$  in contact region conditioned on joint rotation.

Opposite to the hand, we build the object’s deformation field as a rigid motion field,  $T_{\text{R}}$ . For each sampled point inside the object,  $\mathbf{x} \in \mathbf{X}_{\text{obj}}$ , we convert it to object canonical space with the inverse transformation of object pose:

$$T_{\text{R}} = [R_{\text{obj}} \mid t_{\text{obj}}]^{-1} \mathbf{x}, \quad (5)$$

where  $R_{\text{obj}}$  and  $t_{\text{obj}}$  are the rotation and translation in the 6D object pose  $\mathbf{P}_{\text{obj}}$ , respectively.

**Mesh-guided ray sampling.** As mentioned above, since the hand and object follow different motion transformations from observation to canonical space, we need to separate hand and object points in the observation space. However, if we simply follow [44] to leverage the 3D bounding box or 2D segmentation map for separating and sampling points, the hand points will inevitably intersect with the object points due to ambiguity and inaccurate separation. To alleviate this issue, we design a mesh-guided ray sampling scheme, so that hand and object point space will not penetrate each other. Considering the rigid object has a pre-defined shape prior, we could directly constrain sampled points inside the object mesh as the object point set,  $\mathbf{X}_{\text{obj}}$ :

$$\mathbf{X}_{\text{obj}} = \{\mathbf{x} \in \mathcal{HO} \mid \Psi(\mathbf{x}, \mathcal{M}_{\text{obj}}) \leq 0\} \quad (6)$$

where  $\mathcal{M}_{\text{obj}}$  is object mesh, and  $\mathcal{HO}$  denotes the set of all sampling points in the hand-object bounding box.  $\Psi$  indicates whether a point is located outside or inside the given 3D shape. The rest of the points will be viewed as belonging to the hand point set,  $\mathbf{X}_h$ , and will be further constrained by the foreground information reflected from  $\mathbf{W}_c$  to focus on the hand part in the foreground.

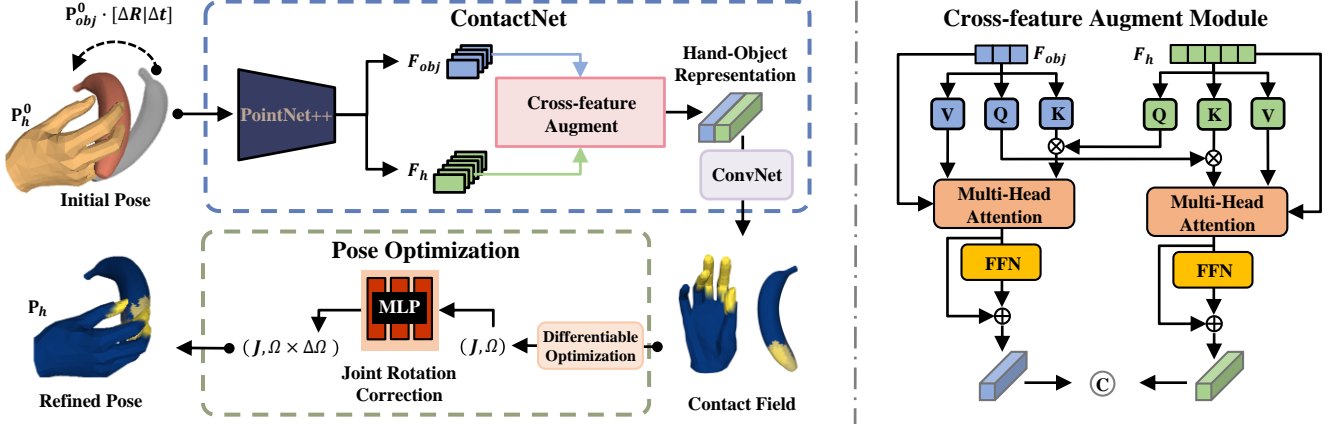


Figure 3. Structure of contact optimization field. Given initial hand-object poses  $P_h^0, P_{obj}^0$ , we first refine object pose by a residual  $\Delta R, \Delta t$  learned from Rigid Pose Correction module (not drawn). Our ContactNet consists of 1) a PointNet++ backbone to extract features for both hand and object, 2) the attention-based cross-feature augment to obtain hand-object interaction representations, and 3) the ConvNet to regress the contact field. The Pose Optimization consists of 1) the Differential Optimization (DiffOpt) module, iteratively updating hand joint and rotation  $(J, \Omega)$  conditional on the contact field, 2) the Joint Rotation Correction module to learn a rotation residual  $\Delta\Omega$ , with which the final refined hand pose is obtained.

### 3.2. Contact Optimization Field

The hand-object pose is of high importance to the hand-object deformation field. Nevertheless, the estimation from the off-the-shelf hand-object estimator is not accurate and thus cannot meet our needs for learning the high-quality dynamic hand-object neural radiance field. Therefore, we leverage contact prior in order to obtain an accurate estimation for the hand-object pose. As shown in Fig. 3, given a hand mesh  $\mathcal{M}_h$  and object mesh  $\mathcal{M}_{obj}$  with initial coarse pose  $\mathbf{P}^0 = \{P_h^0, P_{obj}^0\}$ , we propose the contact optimization field, which first learns to estimate the contact field  $\mathbf{C}$  between hand and object mesh, and further obtain the optimized hand pose  $\mathbf{P}_h$  and object pose  $\mathbf{P}_{obj}$ .

**Rigid object pose correction.** Current contact optimizers, e.g. ContactOpt [11] and TOCH [50], have limited application scope as they only focus on refining hand pose while assuming the ground truth object pose is available or the estimated object pose is accurate. However, such an assumption is not true as either the ground truth object pose is very likely not annotated due to expensive labor work, or the estimated pose for the object could be inaccurate and need further refinement, especially when mutual occlusion is happening. To address this issue, we design a rigid object pose correction module to refine the initial object pose  $\mathbf{P}_{obj}^0$ :

$$\Delta R, \Delta t = \text{MLP}(\mathbf{P}_{obj}^0), \quad (7)$$

where  $\Delta R$  is the residual update of rotation, represented by a 4-dimensional quaternion vector, and  $\Delta t$  is the residual of translation. Both  $\Delta R$  and  $\Delta t$  will then be applied to refine the original object pose:

$$\mathbf{P}_{obj} = \mathbf{P}_{obj}^0 \cdot [\Delta R | \Delta t], \quad (8)$$

Similar to DeepIM [24], our proposed module will iteratively refine the object pose by minimizing the photometric error between rendered image and the observed image. In other words, we jointly train this module with the hand-object neural render, where the photo-metric loss will in return help to refine the object pose in an end-to-end manner.

**ContactNet.** After we refine the object pose, we propose an attention-based network, ContactNet, to estimate the contact field between the hand-object and improve the hand pose estimation jointly, as shown in Fig. 3. The input for this module are coarse hand poses  $\mathbf{P}_h^0$  and refined object pose  $\mathbf{P}_{obj}$  and the output is the contact field:

$$\mathbf{G} = \{\mathbf{G}_h \in \mathbb{R}^{N_h}, \mathbf{G}_{obj} \in \mathbb{R}^{N_{obj}}\}, \quad (9)$$

where  $N_h$  and  $N_{obj}$  are the number of 3D query hand-object points sampled from hand-object mesh surface, respectively. The contact value is normalized to the range  $[0, 1]$ , indicating the probability of whether a query point has a corresponding contact point. Given the sampled hand-object query points, we use PointNet++ [32] to extract hand-object features  $F_h \in \mathbb{R}^{N_h \times 1024}$  and  $F_{obj} \in \mathbb{R}^{N_{obj} \times 1024}$ . Then we apply the cross-feature augment (CFA) module between two features and send the fused hand-object latent representation into a 1-D convolution network to regress the contact value. The structure of CFA module is shown on the right side of Fig. 3, which exploits the interaction between hand and object in the contact region and generates enhanced hand-object representations.

**Hand pose optimization.** Hand pose is then optimized in a differentiable way with obtained contact information. Our

target is to find the hand pose that best complies with contact prior. Firstly, we apply the differentiable optimization (DiffOpt) module to get the contact field  $\mathbf{G}_h$ ,  $\mathbf{G}_{obj}$  based on the corrected hand pose [11]. Secondly, we iteratively minimize the difference between the current contact field and the target contact field and update the hand pose parameters.

The above optimization ensures the grasping is physically-plausible by contact constraints, but there still exists slight misalignment between the optimized pose and the actual one reflected in the image. To bridge this gap, we further employ an MLP to learn a residual  $\Delta\Omega$  for hand joint rotation by leveraging visual constraints. With this joint rotation correction module, the final refined hand pose can be obtained as:

$$\mathbf{P}_h = (J, \Delta\Omega \cdot \Omega, R_h, t_h). \quad (10)$$

where  $J$  are 3D joint locations,  $\Omega$  are local joint rotations, and  $R_h, t_h$  are the hand global rotation and translation, respectively, following the definition in MANO[35].

### 3.3. Training

The NCRF is trained with a photometric reconstruction loss for the estimated color  $\mathbf{C}(\mathbf{r})$  of a ray  $\mathbf{r}$  by rendering the hand-object radiance field using volume rendering, with regard to the ground truth color  $\hat{\mathbf{C}}(\mathbf{r})$ , including VGG-based LPIPS loss [49] and MSE loss [28], with  $\lambda_1 = 0.2$ , under patch-based ray sampling following[44]:

$$\mathcal{L}_{\text{nerf}} = \mathcal{L}_{\text{LPIPS}} + \lambda_1 \mathcal{L}_{\text{MSE}}. \quad (11)$$

The ContactNet is pre-trained on the ContactPose dataset [2] with contact labels gathered from the thermal camera. The contact prediction from the ContactNet will then serve as pseudo label as the target contact map. Then We iteratively optimize the hand pose in the DiffOpt module by minimizing the contact optimization loss:

$$\mathcal{L}_{\text{con}} = |\mathbf{G}_{obj} - \hat{\mathbf{G}}_{obj}| + \lambda_2 |\mathbf{G}_h - \hat{\mathbf{G}}_h|, \quad (12)$$

where  $\hat{\mathbf{G}}_{obj}$  and  $\hat{\mathbf{G}}_h$  are target contact maps.  $\mathbf{G}_{obj}$  and  $\mathbf{G}_h$  are contact maps interpreted from DiffOpt under estimated hand-object pose. We set  $\lambda_2 = 3$ . Besides, we incorporate a collision loss to avoid hand-object interpenetration:

$$\mathcal{L}_{\text{pen}} = \sum_{v \in \mathcal{M}_{obj}} -\min(\text{SDF}_h(v), 0), \quad (13)$$

where  $\text{SDF}_h(\cdot)$  is the signed distance field for the hand to check if any given vertex is inside the hand, and  $v$  represents vertex sampled from object mesh  $\mathcal{M}_{obj}$ . Finally, we obtain the overall objective for jointly optimizing neural rendering and contact optimization:

$$\mathcal{L} = \lambda_{\text{nerf}} \mathcal{L}_{\text{nerf}} + \lambda_{\text{con}} \mathcal{L}_{\text{con}} + \lambda_{\text{pen}} \mathcal{L}_{\text{pen}}. \quad (14)$$

where  $\lambda_{\text{nerf}} = 1$ ,  $\lambda_{\text{con}} = 0.5$ , and  $\lambda_{\text{pen}} = 0.5$  are the loss weights for the corresponding loss.

## 4. Experiments

### 4.1. Datasets and Metrics

**Datasets.** We evaluate our method on HO3D [12] and DexYCB [5] datasets, both of which capture dynamic hand-object interactions from multiple views and provide the annotations. Specifically, DexYCB is captured with 8 cameras, while HO3D is captured by 5 and we are using v3 where the camera poses are provided. To evaluate free-viewpoint rendering, we select multi-view videos with complex hand-object interaction yet enough appearance information. Following the protocol of ZJU-MoCap [31], we take three views for training and leave the remaining views for testing. More details can be found in the supplementary material.

**Metrics.** Similar to preceding neural rendering approaches, we report PSNR, SSIM [43], and LPIPS\* [49] ( $\text{LPIPS}^* = \text{LPIPS} \times 10^3$ ), as the metrics for evaluating rendering quality. Moreover, we report the Mean Per-Joint Position Error (MPJPE) and the Intersection Volume (IV) as the metrics of hand pose estimation and contact optimization, respectively, following ContactOpt [11]. For object pose estimation, we report the metric of ADD-0.1D, which denotes the percentage of average object 3D vertices error within 10% of object diameter.

### 4.2. Comparison with State-of-the-art Methods

**Baselines.** For free-viewpoint rendering, we compare our approach with a SOTA free-view synthesis method, Human-NeRF [44]. In order to adapt it to our task, which is originally designed for neural body rendering, we first train the HumanNeRF based on the MANO for hand modeling and take our object branch for object modeling, and then register the coordinate systems in which two NeRF models align. For hand-object pose estimation, we compare our method with SOTA methods, ContactOpt [11], S<sup>2</sup>Contact [41], and TOCH [50]. All of their results are obtained using the officially released model and code and re-trained under our experiment setting for a fair comparison.

**Comparison on rendering quality.** Given video frames for hand-object interaction, we synthesize novel views and make comparisons on rendering quality. From qualitative results shown in Fig. 4, we can observe that our visual quality is substantially better than HumanNeRF on both HO3D and DexYCB datasets. Although HumanNeRF also embeds a pose correction module to improve the alignment, our method can achieve much better reconstruction results, with the hand-object pose well refined by the designed pose correction module leveraging contact prior, as highlighted in the red circle. Quantitatively, as shown in Table 1, our method outperforms HumanNeRF [44] on all the metrics with a large margin. The result again supports our method is able to achieve the best grasping rendering performance.

**Comparison on pose estimation.** We further compare

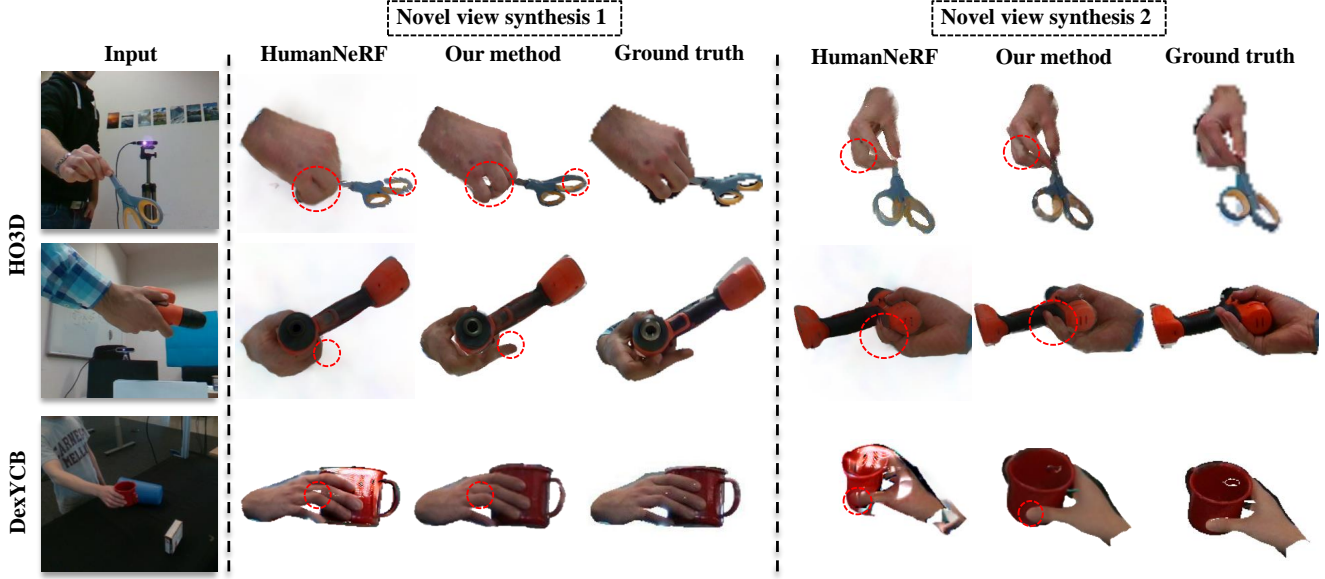


Figure 4. Qualitative comparison with HumanNeRF [44] on the HO3D and DexYCB dataset.



Figure 5. Ablation study on the hand-object neural radiance field consists of non-rigid motion (NR), mesh-guided sampling (MS) and contact optimization field (COF) modules. Zoom in for details.

Table 1. Quantitative results of free-viewpoint rendering on HO3D and DexYCB datasets.

| Datasets | PSNR $\uparrow$ |              | SSIM $\uparrow$ |               | LPIPS* $\downarrow$ |              |
|----------|-----------------|--------------|-----------------|---------------|---------------------|--------------|
|          | HumanNeRF[44]   | Ours         | HumanNeRF[44]   | Ours          | HumanNeRF[44]       | Ours         |
| HO3D     | 26.06           | <b>29.74</b> | 0.9665          | <b>0.9758</b> | 40.23               | <b>32.47</b> |
| DexYCB   | 27.32           | <b>32.16</b> | 0.9719          | <b>0.9813</b> | 27.43               | <b>20.37</b> |

Table 2. Quantitative results of pose estimation on HO3D and DexYCB compared to state-of-the-art approaches.

| Datasets   | Method                      | MPJPE (mm) $\downarrow$ | ADD-0.1D (%) $\uparrow$ | IV (cm $^3$ ) $\downarrow$ |
|------------|-----------------------------|-------------------------|-------------------------|----------------------------|
| HO3D [12]  | Hasson <i>et al.</i> [15]   | 11.4                    | 74.5                    | 9.3                        |
|            | ContactOpt [11]             | 9.5                     | -                       | 8.1                        |
|            | TOCH [50]                   | 9.3                     | -                       | 4.7                        |
|            | S <sup>2</sup> Contact [41] | <b>8.7</b>              | 81.4                    | <b>3.5</b>                 |
|            | Ours                        | 8.9                     | <b>89.8</b>             | 3.7                        |
| DexYCB [5] | S <sup>2</sup> Contact [41] | 11.8                    | 70.5                    | 10.5                       |
|            | Ours                        | <b>10.2</b>             | <b>83.2</b>             | <b>9.3</b>                 |

our method with the state-of-the-art method, S<sup>2</sup>Contact, regarding the performance of hand-object pose estimation, and both methods use the output from the off-the-shelf pose estimator, Hasson *et al.* [15], as the initial pose. As shown in Table 2, we are able to achieve much lower hand pose

error compared to S<sup>2</sup>Contact on Dex YCB dataset while on HO3D, achieving competitive performance on MPJPE and IV metric, and we improve 15.3% and 8.4% on ADD-0.1D metric over the initial pose from Hasson *et al.* [15] and S<sup>2</sup>Contact, respectively. We further include ContactOpt [11] and TOCH [50] as the baselines on HO3D, and again our method achieves the best performance. Both ContactOpt and TOCH suffer the inaccurate object pose annotation, while our method is able to fully optimize the initial coarse hand-object pose, benefiting from both contact optimization and neural rendering.

### 4.3. Ablation Studies

We conduct the ablation study on HO3D dataset. We first explore the effect of different modules in the contact optimization field and hand-object neural radiance field respectively. After that, we analyze the benefit of joint learning contact optimization and neural rendering and the impact of different numbers of camera views.

**Ablation on contact optimization field.** We ablate our full model to study the effect of the contact optimization field, consisting of the cross-feature augment, rigid pose correction, and joint rotation correction module. For cross-

Table 3. Ablation study results of pose estimation.

| Model                         | MPJPE (mm)↓ | ADD-0.1D (%)↑ | IV (cm <sup>3</sup> )↓ |
|-------------------------------|-------------|---------------|------------------------|
| hand-feature augment only     | 9.1         | -             | 3.9                    |
| object-feature augment only   | 9.2         | -             | 4.4                    |
| w/o cross-feature augment     | 9.4         | -             | 5.2                    |
| w/o rigid pose correction     | 10.9        | 74.5          | 5.1                    |
| w/o joint rotation correction | 9.0         | -             | 3.9                    |
| w/o neural rendering          | 9.3         | 74.5          | 4.9                    |
| full model                    | <b>8.9</b>  | <b>89.8</b>   | <b>3.7</b>             |

feature augment, we compare the effect of different feature augment designs. As shown in Table 3, compared to our full model, the hand pose error (MPJPE) increases by 0.3mm and 0.2mm with enhanced hand feature only and the other way around, respectively, and adds up to 0.5mm after removing the whole module. In the ablated version without rigid pose correction, we also observe the hand pose error significantly increases by 2mm, showing that inaccurate object pose will hinder the contact optimization to get the correct hand pose. In the end, ablating the joint rotation correction will result in 0.1mm increment on MPJPE, and the IV error increases by 0.2 cm<sup>3</sup>. Therefore, the ablation study validates the effectiveness of the different modules of the contact optimization field.

**Ablation on hand-object neural radiance field.** We then give the ablation study on the hand-object neural radiance field, where we investigate the effect of the proposed mesh-guided ray sampling and non-rigid deformation field. To validate the usefulness of mesh-guided sampling, we replace it with common 3D bounding box sampling. The first row of Table 4 shows that the superiority of our mesh-guided sampling, *e.g.*, LPIPS\* metric increases by 2.8 after replacement. From the visual comparison (Fig. 5), we observe that the hand appearance will be contaminated by the colors blended from the object due to ambiguity and inaccurate separation without mesh-guided sampling, demonstrating the effective role of mesh-guided sampling in separating hand and object points. Furthermore, disabling non-rigid deformation field introduces a small increase in the LPIPS\* metric by 2.15 (see the second row of Table 4), thus reflecting the improvement brought by the non-rigid deformation field. Similarly, as shown in Fig. 5, adding non-rigid motion can model free-form shape deformation, leading to more plausible grasping rendering.

**Impact of joint learning and camera views.** We study the effect of jointly learning contact optimization and neural rendering. As shown in the second last row in Table 3, the hand error increases by 0.4mm without the help of neural rendering. On the other hand, the performance of novel view synthesis significantly decreases without the help of contact optimization, as shown in the third row of Table 4. We also compare our models trained with different numbers of camera views. The results in Table 4 show that overall

Table 4. Ablation study results of novel view synthesis.

| Model                        | PSNR↑        | SSIM↑         | LPIPS*↓      |
|------------------------------|--------------|---------------|--------------|
| w/o mesh-guided ray sampling | 28.10        | 0.9693        | 35.33        |
| w/o non-rigid motion         | 28.81        | 0.9712        | 34.62        |
| w/o pose optimization field  | 25.71        | 0.9624        | 46.34        |
| with 2 camera views          | 29.57        | 0.9732        | 33.01        |
| with 1 camera view           | 27.93        | 0.9704        | 35.85        |
| full model (3 camera views)  | <b>29.74</b> | <b>0.9758</b> | <b>32.47</b> |

the number of training views improves the performance of novel view synthesis. And it is worth noting that our model can also work effectively under the monocular video setting which is much more challenging.

## 5. Conclusion

In this paper, we propose Neural Contact Radiance Field (NCRF), producing state-of-the-art performances for free-viewpoint renderings of hand-object interaction from a sparse set of videos. Our approach designs a dynamic hand-object neural radiance field capable of modeling challenging hand-object interaction, with complex hand-grasping motions and frequent mutual occlusions. The contact optimization field leverages the contact prior and refines the hand-object pose to comply with the contact constraints and the final image rendering. The refined pose will then drive the proposed hand-object deformation module with the help of mesh-guided sampling to deform rays into the canonical space and render the hand-object interaction photo-realistically. Extensive experiment results on various datasets demonstrate that our approach can achieve state-of-the-art hand-object reconstruction with photo-realistic free-view synthesis.

**Limitations.** Our method has shown state-of-the-art performance in modeling hand-object interaction with photo-realistic appearance. However, our method still has a few limitations. 1) Our method will require the hand and object largely covered under the monocular video setting. 2) We use per-frame pose estimation, thus one following attempt will be applying temporal consistency. 3) We do not consider lighting conditions in this work. The next step will be modeling the environmental lighting conditions and enabling novel lighting synthesis. In summary, these limitations point to a range of exciting avenues for future work.

## 6. Acknowledgements

This work was supported by the Huawei London Research Center (2012 Laboratories), the Institute of Information & communications Technology Planning & Evaluation (IITP) grant funded by the Korean government(MSIT) (No.2022-0-00608, Artificial intelligence research about multi-modal interactions for empathetic conversations with humans).

## References

- [1] ShahRukh Athar, Zexiang Xu, Kalyan Sunkavalli, Eli Shechtman, and Zhixin Shu. RigNeRF: Fully controllable neural 3d portraits. In *CVPR*, 2022. [2](#)
- [2] Samarth Brahmbhatt, Chengcheng Tang, Christopher D Twigg, Charles C Kemp, and James Hays. ContactPose: A dataset of grasps with object contact and hand pose. In *ECCV*, 2020. [6](#)
- [3] Berk Calli, Arjun Singh, Aaron Walsman, Siddhartha Srinivasa, Pieter Abbeel, and Aaron M Dollar. The ycb object and model set: Towards common benchmarks for manipulation research. In *ICAR*, 2015. [1](#)
- [4] Zhe Cao, Ilija Radosavovic, Angjoo Kanazawa, and Jitendra Malik. Reconstructing hand-object interactions in the wild. In *ICCV*, 2021. [1, 2](#)
- [5] Yu-Wei Chao, Wei Yang, Yu Xiang, Pavlo Molchanov, Ankur Handa, Jonathan Tremblay, Yashraj S Narang, Karl Van Wyk, Umar Iqbal, Stan Birchfield, et al. DexYCB: A benchmark for capturing hand grasping of objects. In *CVPR*, 2021. [2, 6, 7](#)
- [6] Xingyu Chen, Baoyuan Wang, and Heung-Yeung Shum. Hand Avatar: Free-pose hand animation and rendering from monocular video. *arXiv preprint arXiv:2211.12782*, 2022. [2, 3](#)
- [7] Zerui Chen, Yana Hasson, Cordelia Schmid, and Ivan Laptev. AlignSDF: Pose-aligned signed distance fields for hand-object reconstruction. In *ECCV*, 2022. [3](#)
- [8] Enric Corona, Tomas Hodan, Minh Vo, Francesc Moreno-Noguer, Chris Sweeney, Richard Newcombe, and Lingni Ma. LISA: Learning implicit shape and appearance of hands. In *CVPR*, 2022. [2, 3](#)
- [9] Bardia Doosti, Shujon Naha, Majid Mirbagheri, and David J Crandall. HOPE-Net: A graph-based model for hand-object pose estimation. In *CVPR*, 2020. [1](#)
- [10] Guillermo Garcia-Hernando, Edward Johns, and Tae-Kyun Kim. Physics-based dexterous manipulations with estimated hand poses and residual reinforcement learning. In *IROS*. IEEE, 2020. [1](#)
- [11] Patrick Grady, Chengcheng Tang, Christopher D. Twigg, Minh Vo, Samarth Brahmbhatt, and Charles C. Kemp. ContactOpt: Optimizing contact to improve grasps. In *CVPR*, 2021. [2, 3, 5, 6, 7](#)
- [12] Shreyas Hampali, Mahdi Rad, Markus Oberweger, and Vincent Lepetit. Honnoteate: A method for 3D annotation of hand and object poses. In *CVPR*, 2020. [2, 6, 7](#)
- [13] Shreyas Hampali, Sayan Deb Sarkar, Mahdi Rad, and Vincent Lepetit. Keypoint transformer: Solving joint identification in challenging hands and object interactions for accurate 3d pose estimation. In *CVPR*, 2022. [2](#)
- [14] Yana Hasson, Gul Varol, Dimitrios Tzionas, Igor Kalevatykh, Michael J Black, Ivan Laptev, and Cordelia Schmid. Learning joint reconstruction of hands and manipulated objects. In *CVPR*, 2019. [1, 2](#)
- [15] Yana Hasson, Bugra Tekin, Federica Bogo, Ivan Laptev, Marc Pollefeys, and Cordelia Schmid. Leveraging photometric consistency over time for sparsely supervised hand-object reconstruction. In *CVPR*, 2020. [1, 2, 3, 7](#)
- [16] Yana Hasson, GÜl Varol, Ivan Laptev, and Cordelia Schmid. Towards unconstrained joint hand-object reconstruction from RGB videos. In *3DV*, 2021. [1](#)
- [17] Markus Höll, Markus Oberweger, Clemens Arth, and Vincent Lepetit. Efficient physics-based implementation for realistic hand-object interaction in virtual reality. In *VR*, 2018. [1](#)
- [18] Yang Hong, Bo Peng, Haiyao Xiao, Ligang Liu, and Juyong Zhang. HeadNeRF: A real-time nerf-based parametric head model. In *CVPR*, 2022. [2](#)
- [19] Hanwen Jiang, Shaowei Liu, Jiashun Wang, and Xiaolong Wang. Hand-object contact consistency reasoning for human grasps generation. In *ICCV*, 2021. [1](#)
- [20] Wei Jiang, Kwang Moo Yi, Golnoosh Samei, Oncel Tuzel, and Anurag Ranjan. Neuman: Neural human radiance field from a single video. In *ECCV*, 2022. [2, 3](#)
- [21] Taein Kwon, Bugra Tekin, Jan Stühmer, Federica Bogo, and Marc Pollefeys. H2O: Two hands manipulating objects for first person interaction recognition. In *ICCV*, 2021. [1](#)
- [22] John P Lewis, Matt Cordner, and Nickson Fong. Pose space deformation: a unified approach to shape interpolation and skeleton-driven deformation. In *Proceedings of the 27th annual conference on Computer graphics and interactive techniques*, 2000. [4](#)
- [23] Kailin Li, Lixin Yang, Xinyu Zhan, Jun Lv, Wenqiang Xu, Jiefeng Li, and Cewu Lu. ArtiBoost: Boosting articulated 3d hand-object pose estimation via online exploration and synthesis. *arXiv preprint arXiv:2109.05488*, 2021. [1, 2](#)
- [24] Yi Li, Gu Wang, Xiangyang Ji, Yu Xiang, and Dieter Fox. DeepIM: Deep iterative matching for 6D pose estimation. In *ECCV*, 2018. [5](#)
- [25] Yuwei Li, Longwen Zhang, Zesong Qiu, Yingwenqi Jiang, Nianyi Li, Yuxin Ma, Yuyao Zhang, Lan Xu, and Jingyi Yu. NIMBLE: a non-rigid hand model with bones and muscles. *ACM Transactions on Graphics (TOG)*, 2022. [2](#)
- [26] Shaowei Liu, Hanwen Jiang, Jiarui Xu, Sifei Liu, and Xiaolong Wang. Semi-supervised 3D hand-object poses estimation with interactions in time. In *CVPR*, 2021. [1, 2, 3](#)
- [27] Marko Mihajlovic, Aayush Bansal, Michael Zollhoefer, Siyu Tang, and Shunsuke Saito. KeypointNeRF: Generalizing image-based volumetric avatars using relative spatial encoding of keypoints. In *ECCV*, 2022. [3](#)
- [28] Ben Mildenhall, Pratul P Srinivasan, Matthew Tancik, Jonathan T Barron, Ravi Ramamoorthi, and Ren Ng. NeRF: Representing scenes as neural radiance fields for view synthesis. In *ECCV*, 2020. [2, 3, 6](#)
- [29] Keunhong Park, Utkarsh Sinha, Jonathan T Barron, Sofien Bouaziz, Dan B Goldman, Steven M Seitz, and Ricardo Martin-Brualla. Nerfies: Deformable neural radiance fields. In *ICCV*, 2021. [3](#)
- [30] Sida Peng, Junting Dong, Qianqian Wang, Shangzhan Zhang, Qing Shuai, Xiaowei Zhou, and Hujun Bao. Animatable neural radiance fields for modeling dynamic human bodies. In *ICCV*, 2021. [2, 3](#)
- [31] Sida Peng, Yuanqing Zhang, Yinghao Xu, Qianqian Wang, Qing Shuai, Hujun Bao, and Xiaowei Zhou. Neural body: Implicit neural representations with structured latent codes for novel view synthesis of dynamic humans. In *CVPR*, 2021. [2, 3, 6](#)

[32] Charles R Qi, Li Yi, Hao Su, and Leonidas J Guibas. PointNet++: Deep hierarchical feature learning on point sets in a metric space. In *NeurIPS*, 2017. 5

[33] Xun Qian, Fengming He, Xiyun Hu, Tianyi Wang, and Karthik Ramani. Arnnotate: An augmented reality interface for collecting custom dataset of 3d hand-object interaction pose estimation. In *Proceedings of the 35th Annual ACM Symposium on User Interface Software and Technology*, 2022. 1

[34] Yuzhe Qin, Yueh-Hua Wu, Shaowei Liu, Hanwen Jiang, Ruihan Yang, Yang Fu, and Xiaolong Wang. Dexmv: Imitation learning for dexterous manipulation from human videos. In *ECCV*, pages 570–587, 2022. 1

[35] Javier Romero, Dimitrios Tzionas, and Michael J Black. Embodied hands: Modeling and capturing hands and bodies together. *ACM Transactions on Graphics (ToG)*, 2017. 1, 2, 4, 6

[36] Srinath Sridhar, Anna Maria Feit, Christian Theobalt, and Antti Oulasvirta. Investigating the dexterity of multi-finger input for mid-air text entry. In *Proceedings of the 33rd Annual ACM Conference on Human Factors in Computing Systems*, 2015. 1

[37] Shih-Yang Su, Frank Yu, Michael Zollhöfer, and Helge Rhodin. A-nerf: Articulated neural radiance fields for learning human shape, appearance, and pose. *Advances in Neural Information Processing Systems*, 34:12278–12291, 2021. 2, 3

[38] Gusi Te, Xiu Li, Xiao Li, Jinglu Wang, Wei Hu, and Yan Lu. Neural capture of animatable 3d human from monocular video. In *ECCV*, 2022. 2, 3

[39] Bugra Tekin, Federica Bogo, and Marc Pollefeys. H+O: Unified egocentric recognition of 3D hand-object poses and interactions. In *CVPR*, 2019. 1

[40] Tze Ho Elden Tse, Kwang In Kim, Ales Leonardis, and Hyung Jin Chang. Collaborative learning for hand and object reconstruction with attention-guided graph convolution. In *CVPR*, 2022. 3

[41] Tze Ho Elden Tse, Zhongqun Zhang, Kwang In Kim, Ales Leonardis, Feng Zheng, and Hyung Jin Chang. S2Contact: Graph-based network for 3d hand-object contact estimation with semi-supervised learning. In *ECCV*, 2022. 2, 3, 6, 7

[42] Etsuko Ueda, Yoshio Matsumoto, Masakazu Imai, and Tsukasa Ogasawara. A hand-pose estimation for vision-based human interfaces. *IEEE Transactions on Industrial Electronics*, 2003. 1

[43] Zhou Wang, Alan C Bovik, Hamid R Sheikh, and Eero P Simoncelli. Image quality assessment: from error visibility to structural similarity. In *TIP*, 2004. 6

[44] Chung-Yi Weng, Brian Curless, Pratul P Srinivasan, Jonathan T Barron, and Ira Kemelmacher-Shlizerman. HumanNerf: Free-viewpoint rendering of moving people from monocular video. In *CVPR*, 2022. 2, 3, 4, 6, 7

[45] Yuelang Xu, Lizhen Wang, Xiaochen Zhao, Hongwen Zhang, and Yebin Liu. ManVatar: Fast 3d head avatar reconstruction using motion-aware neural voxels. *arXiv preprint arXiv:2211.13206*, 2022. 2

[46] Lixin Yang, Xinyu Zhan, Kailin Li, Wenqiang Xu, Jiefeng Li, and Cewu Lu. CPF: Learning a contact potential field to model the hand-object interaction. In *ICCV*, 2021. 1, 2

[47] Yufei Ye, Abhinav Gupta, and Shubham Tulsiani. What's in your hands? 3d reconstruction of generic objects in hands. In *CVPR*, 2022. 3

[48] Ziwei Yu, Linlin Yang, You Xie, Ping Chen, and Angela Yao. Uv-based 3d hand-object reconstruction with grasp optimization. *arXiv preprint arXiv:2211.13429*, 2022. 2

[49] Richard Zhang, Phillip Isola, Alexei A Efros, Eli Shechtman, and Oliver Wang. The unreasonable effectiveness of deep features as a perceptual metric. In *CVPR*, 2018. 6

[50] Keyang Zhou, Bharat Lal Bhatnagar, Jan Eric Lenssen, and Gerard Pons-Moll. TOCH: Spatio-temporal object-to-hand correspondence for motion refinement. In *ECCV*, 2022. 2, 3, 5, 6, 7